Effect of Digestion Time on Size and Magnetic Properties of Spinel CoFe 2 O 4 Nanoparticles

ARTICLE *in* THE JOURNAL OF PHYSICAL CHEMISTRY C · JANUARY 2009

Impact Factor: 4.77 · DOI: 10.1021/jp8083875

3 AUTHORS, INCLUDING:

Ayyappan Sathya
Istituto Italiano di Tecnologia
15 PUBLICATIONS **360** CITATIONS
SEE PROFILE

John Philip
Indira Gandhi Centre for Atomic Research
179 PUBLICATIONS **3,149** CITATIONS
SEE PROFILE

THE JOURNAL OF PHYSICAL CHEMISTRY C

Article

Effect of Digestion Time on Size and Magnetic Properties of Spinel CoFeO Nanoparticles

S. Ayyappan, John Philip, and Baldev Raj

J. Phys. Chem. C, **2009**, 113 (2), 590-596 • Publication Date (Web): 19 December 2008

Effect of Digestion Time on Size and Magnetic Properties of Spinel $CoFe_2O_4$ Nanoparticles

S. Ayyappan, John Philip,* and Baldev Raj

SMARTS, NDED, Metallurgy and Materials Group, Indira Gandhi Centre for Atomic Research, Kalpakkam 603 102, Tamilnadu, India

Received: September 21, 2008; Revised Manuscript Received: November 18, 2008

We investigate the effect of digestion time on size, distribution, and magnetic properties of $CoFe_2O_4$ nanoparticles prepared by the precipitation approach. The average crystalline size increases from 14 to 19 nm as the digestion time is increased from 1 to 120 min. The observed dependence of average particle size with digestion time is in good agreement with Lifshitz, Slyozov, and Wagner theory. Our results suggest that the dissolution of $Co^{2+}-Fe^{3+}$ complexes form the surface followed by crystallization of spinel oxide through Oswald ripening process. This observation is in sharp contrast to the growth process in Fe_3O_4 nanoparticles where Oswald ripening is insignificant beyond 5 min due to the electron hopping between Fe^{2+} and Fe^{3+} ions. Magnetization measurements show that the saturation magnetization value decreases from 60 to 49 emu/g as the digestion time is increased from 1 to 120 min. Raman and Mossbauer spectroscopic investigations reveal that reduction of magnetization with increasing particle size is due to the formation of nonmagnetic ferrihydrite at higher digestion times.

Introduction

There has been a growing interest in nanoparticles, nanosheets, nanowires, nanotubes, and quantum dots due to their potential application in various fields.[1−6] It has been known for quite some time that the physical and chemical properties of nanoscale materials are different from the bulk solids.[7,8] Among various nanoscale materials, transition metal oxide nanoparticles with spinel structure have attracted considerable interest due to their remarkable optical, electronic, mechanical, thermal, and magnetic properties. These properties are exploited in technological applications like ferrofluid, biomedicine, and recording media.[9−14] Ferrofluids and their emulsions are easy to manipulate with external magnetic field and hence extensively used for various technological applications[15,16] and fundamental studies.[17] Spinel ferrites are magnetic materials with a general formula $(M_\delta Fe_{1-\delta})[M_{1-\delta}Fe_{1+\delta}]O_4$. Here, δ is the cation distribution factor, which illustrates the fraction of tetrahedral (A-) sites occupied by divalent metal (M^{2+}) cations. The round and square brackets denote the tetrahedral (A-) and octahedral (B-) interstitial sites, M is the divalent (Mn^{2+}, Fe^{2+}, Co^{2+}, Ni^{2+}, Zn^{2+}, etc.), and Fe is the trivalent (Fe^{3+}) metal cation occupying the fcc lattice formed by O^{2-} anions.[18] $\delta = 1$ is "normal" spinel, with all the divalent (M) cations on the tetrahedral (A-) sites and the trivalent (Fe^{3+}) cations on the octahedral (B-) sites, which can be represented by the formula $(M)[Fe^{3+}Fe^{3+}]O_4$. $\delta = 0$ is "inverse" spinel, $(Fe^{3+})[MFe^{3+}]O_4$, in which the divalent cations occupy the B-sites and the trivalent cations are equally divided among the A- and remaining B-sites. The magnetic properties of a spinel is sensitive to the type of cations and their distribution among the two interstitial sites of spinel lattice and the relative strength of inter (J_{AB}) and intra sublattice (J_{AA} or J_{BB}) interactions. For example, $ZnFe_2O_4$ is a normal spinel with the Zn^{2+} ions at the A-site and the Fe^{3+} ions at the B-site. Thus, $ZnFe_2O_4$ exhibits lower magnetic moment (~5 emu/g) at room temperature. However, $ZnFe_2O_4$ becomes magnetically ordered with a large magnetic moment even (~62 emu/g at room temperature) if vacuum thermal annealed at 1000 °C and cooled to room temperature. The observed high magnetic ordering is attributed to the change in the cation distribution from the normal to mixed spinel type, where Fe^{3+} and Zn^{2+} occupies both sites under vacuum thermal annealing.[19] The cation distribution between A- and B-site depends on the ionic radii and the type of bonding and the preparation method. The distribution can be changed by changing the temperature, pressure, magnetocrystalline anisotropy, and composition of metal ions.[20,21] $CoFe_2O_4$ is typically an inverse spinel having a formula of $(Co_\delta Fe_{1-\delta})[Co_{1-\delta}Fe_{1+\delta}]O_4$ with $\delta = 0$.[22] Since Fe^{3+} ions are occupied equally, with their spin in the opposite direction, in the A- and B-sites, the magnetic property is mainly dependent on the Co^{2+} ions ($3d^7$) that has an orbital moment of 3.7 μ_B per formula unit.[18] $CoFe_2O_4$ is unique among the spinel structure ferrites because of its large magnetic anisotropy (ranging from 8×10^6 to 3.15×10^7 erg/cm^3), large magnetostriction, reasonable saturation magnetization ($M_s \approx 80$ emu/g), high coercivity (5.1 kOe), high chemical stability, and site specific and strong binding nature to serum albumin proteins compared to magnetite nanoparticles.[22−27] Therefore, $CoFe_2O_4$ nanoparticles are ideal candidates for magneto-optic recording media, data storage, high-frequency, and biomedical applications.[28−30]

Tailoring $CoFe_2O_4$ nanoparticles of desired size, magnetic properties, and chemical purity has been attempted by different synthesis routes such as chemical reduction, sonochemical, Langmuir−Blodgett technique, sol−gel, combustion reaction, microemulsion, seed mediated growth, hydrothermal, mechanical milling, and coprecipitation.[31−37] Among these methods, coprecipitation is one of the easy and versatile techniques, which involves simultaneous occurrence of nucleation and growth. Growth of nucleated particles dramatically changes the particle size, morphology, and final product.[38] The particle growth is influenced by pH, solubility of ions, and secondary growth process such as Oswald ripening and aggregation.[39,40] In coprecipitation, any additives lead to decrease the surface tension of the nucleated particles and hence the growth of the particles can be controlled by the addition of a suitable surfactant.

* Corresponding author. E-mail: philip@igcar.gov.in.

10.1021/jp8083875 CCC: $40.75
Published on Web 12/19/2008

Coarsening involves growth of larger particles at the expense of smaller particles (also known as Oswald ripening). An understanding of the growth process is a prerequisite to tune the nanoparticles of desired size and properties. Ostwald ripening is often monitored in solution phase synthesis by many groups.[41−47] Oskam et.al. studied the time and temperature dependent size and distribution of TiO_2 nanoparticles.[47] The aging effect studies up to 24 h on the size distribution of Fe_3O_4 nanoparticles synthesized by solvothermal technique confirm that the growth process is diffusion-limited.[41] Studies on Fe_3O_4 nanoparticles, synthesized by the chemical method, show insignificant Oswald ripening beyond a digestion time of 5 min, due to the electron hopping between Fe^{2+} and Fe^{3+} that drives the cubic spinel phase formation.[37] The above studies show that the ripening process depends on the ferrite system, cations, initial precursors, and synthesis method. There has been no report on the effect of digestion time on the growth process in cobalt ferrite. In this paper, we investigate the effect of digestion time on size, distribution, impurity formation, and magnetic properties of $CoFe_2O_4$ nanoparticles. Further, the reason for the decrease in magnetization with increase in particle size in ferrites remains a long pending puzzle. Raman spectroscopic studies show that the reduction in the magnetization with increasing particle size is due to the presence of the nonmagnetic ferrihydrite phase.

Experimental Methods

Preparation Method. $CoFe_2O_4$ nanoparticles were prepared by the precipitation method.[37] $FeCl_3 \cdot 6H_2O$ (2 M) and $CoCl_2 \cdot 6H_2O$ (1 M) salt solutions were freshly prepared in water medium. These salt solutions were mixed in 1:1 ratio with a continuous stirring speed of 1000 rpm at 90 °C, pH 1.5. $CoFe_2O_4$ nanoparticles were obtained by addition of 6 N NaOH in the above-mentioned salt solution at the rate of 10 mL/s. after the addition of alkali, the pH reached a value of 12. At this stage, the solution turned to black, indicating the formation of $CoFe_2O_4$ nanoparticles. The same pH, temperature, and stirring speed were maintained for different digestion times (1, 2, 5, 15, 30, 60, and 120 min). After each digestion time, 6 mL of oleic acid was added to the above solution to coat the particles as well as restrict the particle growth process. The oleic acid was added at the relatively low temperature of 70 °C and the mixture was left for 30 min. Later, particles were acidified with dilute hydrochloric acid (HCl) to separate particles from the dispersion. The top water layer with salt impurities was discarded. The above obtained surfactant coated particles were washed with Elga water at 60 °C, until the water pH reached a value of 7, to remove ionic salt impurities trapped or adhering to the particles coagulum. The water-washed particles were dispersed in hexane. The hexane dispersion was treated with acetone to induce aggregation of particles. The aggregated particles were separated by centrifugation at 2500 rpm for 30 min. Addition of acetone to hexane increases the dielectric constant of the medium, which led to aggregation and sedimentation of particles dispersed in hexane. However, excess acetone and repeated acetone wash also caused desorption of oleic acid from the $CoFe_2O_4$ interface, due to the competition between the affinity of the carboxylate group of the oleic acid to the surface of the $CoFe_2O_4$ particles and the organic polar solvent (acetone/hexane mixture). The washing procedure was repeated two times to eliminate excess free surfactant molecules. Oleic acid-coated $CoFe_2O_4$ particles were dried at 35 °C for 24 h in inert atmosphere. These dried powders were used for further characterization.

Characterization. The sample crystallographic properties and average particle size were determined by a MAC Science MXP18 X-ray diffractometer. 2θ values were taken from 15° to 65°, using Cu Kα radiation (λ value of 1.546 Å). The X-ray diffraction (XRD) patterns of nanoparticles were verified by comparing with the JCPDS card no. 22-1086. High-resolution transmission electron microscopy (HRTEM) investigations were carried out with use of a JEOL 2000 EX II (T) operated at 200 kV. One drop of a colloidal suspension of $CoFe_2O_4$ in hexane was collected on a carbon film coated copper grid, then dried overnight under a lamp. Raman spectra were recorded with a HR800 (Jobin Yvon) microspectrometer. A small quantity of the sample was placed in a glass slide on the microscopy stage. A 514 nm Ar ion laser was used for excitation of the sample. Power incident on the sample surface was about 0.5 mW, with a laser spot size of about 1.5 μm with 100× objective. Dispersion of the Raman scattering was achieved through prism and an 1800 gr/mm grating. Data acquisition was done in the range 2000−100 cm^{-1} from the laser line for 30 s. The magnetic properties of the $CoFe_2O_4$ nanoparticle are studied by using a Vibrating sample magnetometer (EG&G PRINCETON Model: 4500) and Mossbauer spectroscopy. Room temperature magnetization measurements of $CoFe_2O_4$ nanoparticles were carried out with the applied magnetic field range of ±7 kOe. A Mossbauer spectrum was recorded on $CoFe_2O_4$ nanoparticle, using an electromechanical type spectrometer with constant acceleration mode. A source of ^{57}Co(Rh) held at room temperature was used. The Mossbauer spectra of the samples were fitted with a Lorentzian-shaped line by the method of least squares. The isomer shift values reported in this paper are with respect to α-Fe at room temperature.

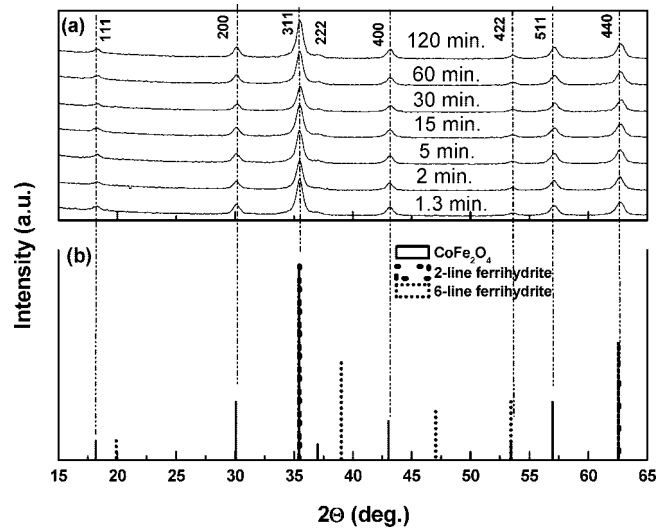

Figure 1. (a) Powder diffraction pattern of $CoFe_2O_4$ nanoparticles synthesized at different digestion times. (b) Peaks of $CoFe_2O_4$ (solid line), 2-line ferrihydride (dash line), and 6-line ferrihydride (doted line) of standard patterns. Vertical lines (dash dot dot) represent diffraction peaks that are matched with $CoFe_2O_4$.

Results and Discussion

A. XRD and TEM Analysis. Figure 1 shows the XRD spectrum of $CoFe_2O_4$ prepared at different digestion times. The characteristic peaks are compared with those of $CoFe_2O_4$, 2-line ferrihydrite, and 6-line ferrihydrite standard peaks. The highly crystalline peaks can be matched with the Bragg reflections (220), (311), (222), (400), (422), (511), and (440) planes corresponding to the standard patterns of JCPDS card no. 22-1086. The phase shows the pure cubic structure of $CoFe_2O_4$ ($Fd3m$, a = 8.391 Å). All the observed peaks become sharper

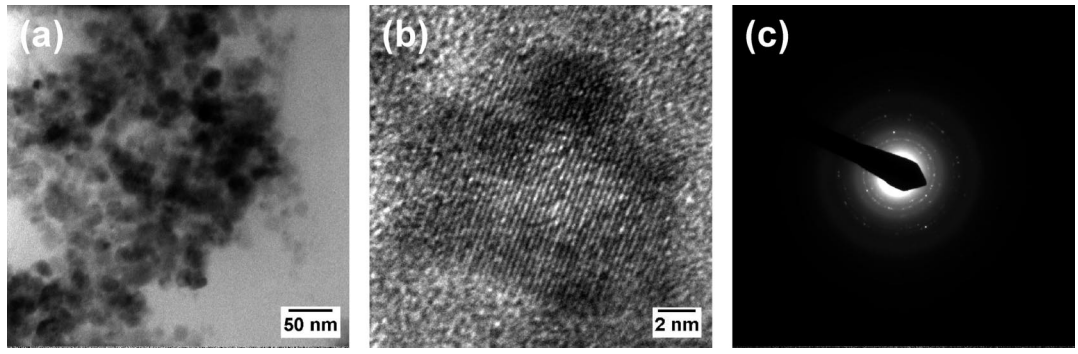

Figure 2. (a) TEM image of $CoFe_2O_4$ nanocrystals synthesized at the digestion time of 15 min. (b) HRTEM lattice image from a single $CoFe_2O_4$ nanocrystallite. (c) Selected area electron diffraction (SAED) of the specimen showing diffuse rings from $CoFe_2O_4$ reflections.

and intense as the digestion time increases from 1 to 120 min. The average particle size of the nanoparticle is determined from the broadening of the most intense peak (311) in the XRD pattern, using the Debye−Scherrer formula. TEM analysis is also used to find the exact particle size and interplanar distance. The average particle size obtained at digestion times of 1.3, 2, 5, 15, 30, 60, and 120 min are 13.9, 14.4, 15, 15.5, 16, 17, and 19 nm, respectively. The lattice parameter value obtained in all cases is 8.378 Å, which is in good agreement with the standard value of 8.391 Å. Figure 2a shows the transmission electron microscopy (TEM) image of $CoFe_2O_4$ nanoparticles synthesized at a digestion time of 15 min. The average diameter obtained from image analysis is 14.81 nm, against the value of 15 nm obtained by XRD. Panels b and c of Figure 2 show high-resolution TEM (HRTEM) and selected area electron diffraction (SAED) pattern, respectively. The clear lattice boundary in the HRTEM image illustrates the high crystallinity of $CoFe_2O_4$ nanoparticles (Figure 2b). The periodic fringe spacing of 0.26 nm corresponds to the (311) plane of cubic $CoFe_2O_4$. The SAED pattern shows the diffuse rings with less intensity, which can be indexed to $CoFe_2O_4$ [(220), (311), (400), (422), (511), and (440) planes] reflections.

In a precipitation technique, nucleation begins in a supersaturation solution, depending on the interfacial energy (σ), volume of the particles (v), and thermal energy (k_BT). The equilibrium critical radius, r^*, is given by

$$r^* = \frac{2v\sigma}{k_BT\ln(S)} \quad (1)$$

In general, the nucleation occurs when the supersaturation (S) reaches a certain value above the solubility, which is the energy barrier for the formation of nuclei. After the initial nucleation, the Gibbs free energy for the formation of nuclei reduces due to the decrease in concentration of reactants. When it decreases below a specific concentration (critical energy for nucleation), no more nuclei can form. However, particle growth can continue through molecular addition until the concentration of the precipitated species reaches an equilibrium concentration. However, in case of $r > r^*$ smaller particles grow more rapidly than the larger ones because smaller particles have more free energy driving force compared to larger ones. At this stage, nearly monodisperse size distribution can be obtained by stopping the reaction. On the other hand, the ripening process occurs when the reactants reduce, resulting in an increase in the critical nuclei size (r^*) due to a decrease in the supersaturation ratio (S). It is known that any particle smaller than the new critical radius will dissolve and redeposit on existing particles. Therefore, smaller particles disappear with time, and the larger particles continue to grow. If the reaction is stopped

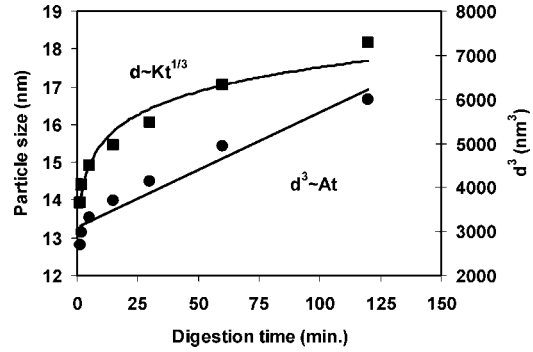

Figure 3. Average particle size (circle, left axis) and the cube of the average particle size (square, right axis) of $CoFe_2O_4$ nanoparticles as a function of digestion time. The solid lines show the best fit of $d \approx (Kt)^{1/3}$ and $d^3 \approx At$.

at this stage before reaching equilibrium, particles will have a broad size distribution. Since the ripening process occurs at very low supersaturation, it can be controlled by surface reaction that has a dominant effect. Any additives (such as surfactants) to the system can slow down the surface reaction step and can automatically terminate the Oswald ripening process and stabilize the particle growth. In addition to the growth by molecular addition, the particles can also grow by aggregation with other smaller unstable particles through secondary growth. The rate of particle growth by aggregation is much larger than that of molecular addition. However, most of the nanoparticles are not thermodynamically stable due to high surface energy. Therefore, to produce stable nanoparticles, the growth must be arrested during chemical reaction by adding surface protecting reagents. The growth of larger particles at the expense of smaller particles is known as Oswald ripening or dissolution−crystallization. A detailed mathematical description of Ostwald ripening was first developed by Lifshitz and Slyozov and also independently by Wagner, and their combined models are referred to as LSW theory.[48] In $CoFe_2O_4$ precipitation, Co^{2+}−Fe^{3+} complexes form the surface, followed by crystallization of spinel oxide by Oswald ripening. This process takes place with considerable particle growth. Final chemical reaction is given by

$$2Fe^{3+} + Co^{2+} + 8OH^- \rightarrow CoFe_2O_4 + 4H_2O \quad (2)$$

Figure 3 shows the average particle size and cube of the average particle size versus digestion time. The average particle size increases from 14 to 19 nm as the digestion time increases from 1 to 120 min. The cube of average particle size increases linearly with digestion time, which is in good agreement with the Lifshitz−Slyozov−Wagner (LSW) model for coarsening. The

solid lines show the best fits obtained by using the equations $d \approx (Kt)^{1/3}$ and $d^3 \approx At$.

It has been shown that the Lifshitz−Slyozov−Wagner (LSW) theory provides a quantitative treatment of the time dependence of the particle growth.[47] Coarsening is driven by the dependence of the solubility of a solid phase on the particle size. For spherical particles, the solubility c_r of a particle of radius r is given by

$$c_r = c_\infty \exp\left(\frac{2\gamma V_m}{RT}\frac{1}{r}\right) \quad (3)$$

where c_∞ is the solubility at a flat surface, V_m is the molar volume, γ is the surface energy of the solid, R is the gas constant, and T is the temperature. When $(2\gamma V_m/rRT) < 1$, the exponential term in eq 3 can be linear. Assuming that the growth rate is determined by diffusion of the solute from the smaller particles to the larger particles

$$\vec{r}^3 - \vec{r}_0^3 = \frac{8\gamma D V_m^2 c_\infty}{9RT} t = At \quad (4)$$

where $\vec{r}$ is the average particle size at time t, A is the constant and $\vec{r}_0$ is the average particle size at time zero. Our observation of the linearity of particle size with time (Figure 3) suggests that the increase in particle size is dominated by diffusion-limited growth through out the digestion time (1−120 min). The best linear fit in Figure 3 gives an A value of 30. Earlier studies on magnetite particles show that the growth is finished within 5 min, above which Oswald ripening is insignificant due to high electron mobility between Fe^{2+} and Fe^{3+} ions that drives a local cubic close packed ordering at higher digestion time.[37] However, in the case of $CoFe_2O_4$ nanoparticle, $Co^{2+}-Fe^{3+}$ complexes form the surface, followed by crystallization of spinel oxide by ripening. Therefore, the growth process continues for a long time. Study on the digestion effect in MnO nanocrystals, synthesized by thermal decomposition, shows that the particles growth process is diffusion limited and continues up to 60 min.[46] Similar results are obtained in the growth of the TiO_2 nanoparticles up to 125 h at 200 °C.[47]

It is known that rapid hydrolysis of Fe(III) solutions leads to the formation of ferrihydrite. Modest heating of the Fe(III) solutions at 80 °C typically produces 6-line ferrihydrite, whereas the 2-line variety is produced at ambient temperatures by the addition of alkali to raise the pH to about 7.[49] However, during $CoFe_2O_4$ nanoparticles precipitation, there is the possibility that an adequate amount Fe^{3+} solution may be turned into the ferrihydrite phase by the rapid addition of 6 N NaOH at 90 °C. Drits et al. obtained an X-ray pattern for 2-line ferrihydrite, where they observed two peaks at 2.59 and 1.48 Å d spacing, corresponding two θ values of 35.43° and 65.58°.[50] Peaks of 2-line ferrihydrite overlap with those corresponding to the $CoFe_2O_4$ phase. The standard 2-line and 6-line ferrihyhydrite phases cannot be distinguished from the $CoFe_2O_4$ phase from the XRD pattern. Therefore, the Raman spectrum is employed to check the presence of ferrihydrite in the $CoFe_2O_4$ nanoparticles synthesized at different digestion times.

B. Raman Studies. Raman spectroscopy is highly sensitive and uniquely suitable for many lattice effects, such as structure transition, lattice distortion, charge−lattice and spin−lattice couplings, local cation distribution, and magnetic ordering.[51,52] Therefore, Raman spectroscopy is one of the powerful techniques for a direct probe of lattice dynamics and cation migration in any spinel ferrite. $CoFe_2O_4$ has inverse cubic spinel structure belonging to the space group O_h^7 ($Fd3m$). The full unit cell contains 56 atoms but the smallest Bravais cell contains only

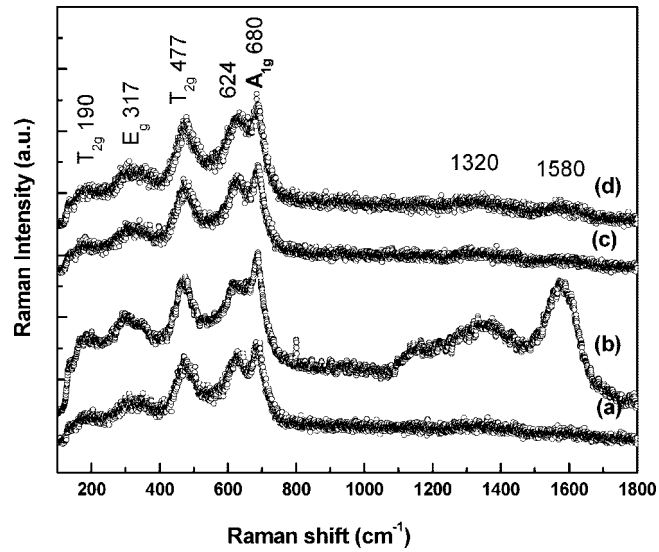

Figure 4. The room temperature Raman spectra of $CoFe_2O_4$ synthesized at different digestion times of (a) 1, (b) 5, (c) 15, and (d) 120 min.

14 atoms. Therefore, 42 vibrational modes are possible. Group theory predicts five Raman active modes ($A_{1g} + E_g + 3T_{2g}$) composed of the motion of O ions and both the A- and B-site ions.[53] Raman spectra of $CoFe_2O_4$ nanoparticles, prepared at different digestion times (1, 5, 15, and 120 min), are shown in Figure 4. Room temperature Raman spectra at different digestion times of 1, 5, 15, and 120 min consist of broad bands at ∼190, ∼306, ∼477, 1320, and 1580 cm^{-1}, and strong bands at ∼630 and ∼690 cm^{-1} in the frequency range of 100−2000 cm^{-1}. The best curve fitting on the spectra with use of Lorantzian shaped lines reveals four peak positions of Raman spectra. All the observed peaks are similar to the bulk maghemite phase, except one of the B-sites T_{2g} mode at 585 cm^{-1}. All the observed peaks are shifted to the lower wavenumber owing to the higher mass of Co compared to Fe. The peaks at ∼190 and ∼306 cm^{-1} illustrate the T_{2g} and E_g modes, respectively.[50] The peak at ∼477 is assigned to the T_{2g} mode corresponding to the local lattice vibrations of Fe^{3+} and O^{2-} in the octahedral site of the $CoFe_2O_4$ phase. We observed two strong bands at ∼630 and ∼690 cm^{-1} against the reported single band value of ∼651 cm^{-1} for A_{1g} stretching vibrations of Fe^{3+} and O^{2-} in the tetrahedral site of the $CoFe_2O_4$ phase or the 710 cm^{-1} band of 2-line ferrihydrite. It has been reported that the occurrence of bands at 650, 330, and 300 cm^{-1}, in both the Raman and IR spectra, would depend on the A and E components into which the T_{2g} and T_{1u} (IR active mode) species are resolved on reduction of symmetry.[54] Apart from four optical phonon modes, there exists one peak at 1320 cm^{-1} for 1 min digestion time corresponding to the ferrihydrite phase. At higher digestion times (5, 15, and 120 min), one more peak arises at around 1580 cm^{-1} along with that at 1320 cm^{-1}. It has been reported that the bands at 1320 and 1580 cm^{-1} in Raman spectra are assigned to ferrihydrite, as well as γ-Fe_2O_3 phases. Janney et al. have reported that the bands at 1320 and 1580 cm^{-1} are due the magnetite-like modification of ferrihydrite.[55] It has also been reported in the literature that the bands at 1320 and 1580 cm^{-1} correspond to maghemite.[56] It appears that during higher digestion time, a small amount of the ferrihydrite phase, which is nonmagnetic in nature, is formed during $CoFe_2O_4$ synthesis. Formation of ferrihydrite decreases the symmetry in the B-site that results in the doublet at 650−700 cm^{-1}. The presence of small amounts of ferrihydrite and γ-Fe_2O_3 phases cannot be detected by XRD

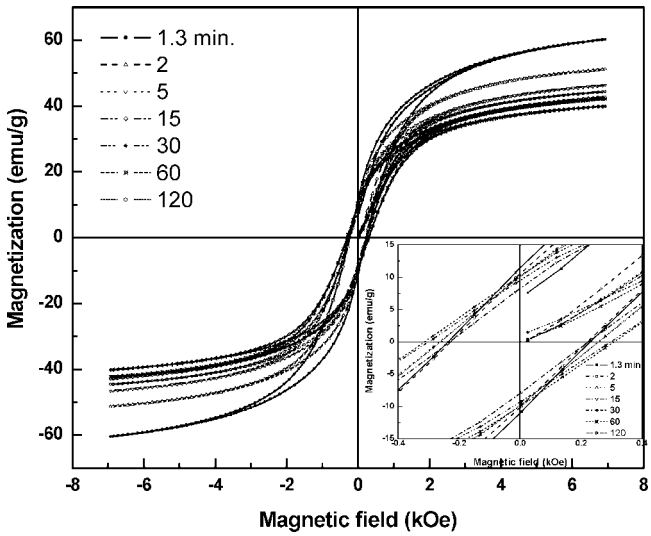

Figure 5. Room temperature hysteresis loops of $CoFe_2O_4$ nanoparticles synthesized at different digestion times of 1, 2, 5, 15, 30, 60, and 120 min. Inset: Enlarged version of the hysteresis loop up to ±0.4 kOe magnetic field showing the variation of coercive field and remanent values.

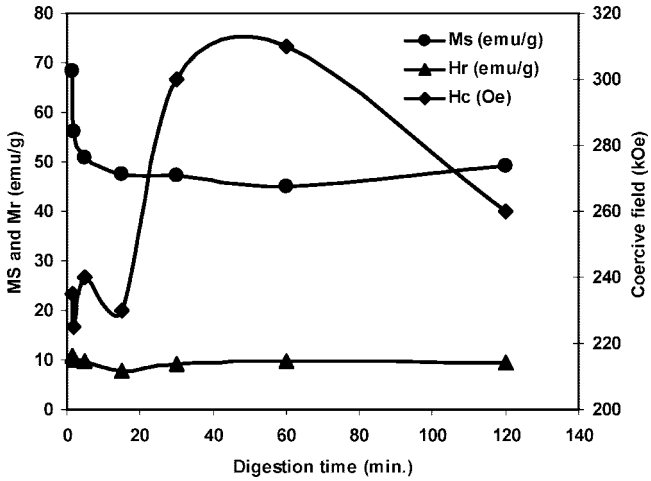

Figure 6. Saturation magnetization (circle, left axis) and magnetic remanance (triangle, left axis) and coercive field (square, right axis) measured at 300 K for $CoFe_2O_4$ nanoparticles as a function of digestion time.

analysis because the most intense peak position of both phases is identical as shown in Figure 1. Magnetization measurements are utilized to probe the influence of ferrihydrite formation during $CoFe_2O_4$ precipitation.

C. Magnetization Measurements. Figure 5 shows the room temperature magnetization loops of $CoFe_2O_4$ synthesized at different digestion times in the magnetic field range of ±7 kOe. Hysterisis loops show that $CoFe_2O_4$ synthesized at different digestion times depicts ferromagnetic behavior with finite coercivity between 250 and 300 Oe. Figure 6 shows digestion time versus saturation magnetization (Ms), remanance magnetization (Mr), and coercivity (Hc) values. It is observed that the saturation magnetization (Ms) value for 1.3 min is 60 emu/g, which is 75% of the bulk value. In the case of 120 min digestion time, the Ms is 49.26 emu/g corresponding to 61% of bulk value. At 30 min, Ms reaches a minimum of 40 emu/g corresponding to 50% of bulk value. There is no change in Hc up to 15 min and the average value is 250 Oe. At higher digestion times, from 30 to 60 min, the Coercivity varies from 300 to 310 Oe and finally it drops to 260 Oe, with a saturation

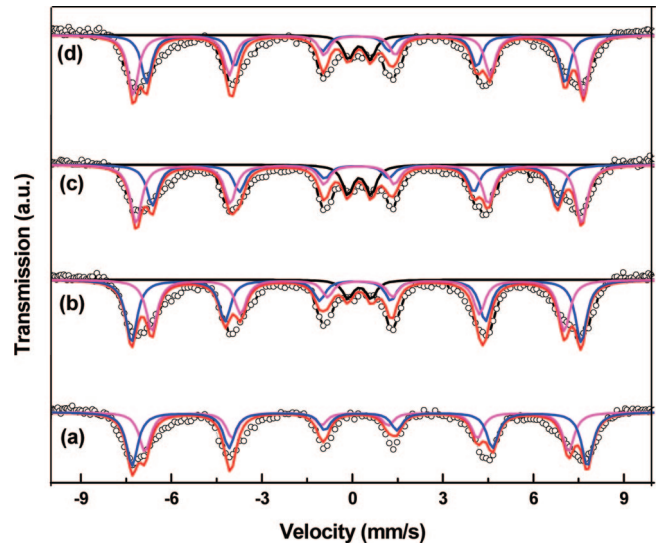

Figure 7. Room temperature Mossbauer spectra of the $CoFe_2O_4$ nanoparticles prepared at different digestion times of (a) 1, (b) 5, (c) 15, and (d) 120 min.

magnetization (Ms) value of 49.26 emu/g, at the digestion time of 120 min. Remanance magnetization initially decreases (from 10 to 7.7 emu/g) up to 15 min and reaches 9.5 emu/g at 120 min. Since all the samples are prepared under identical conditions, the decrease in saturation magnetization values can only be attributed to the nonmagnetic ferrihydrite formation. Reduction in saturation magnetization with increasing size in magnetic nanoparticle system remains as a controversial issue.[57] The studies in NiO antiferromagnetic nanoparticles in the size range 5 to 80 nm showed anomalous magnetic properties that are attributed to the uncompensated surface spins that are induced by the broken exchange bonds at the surface of the magnetic nanoparticles. Oxygen vacancies can break the superexchange paths and induce spin disorder during milling.[58] The nonmagnetic shell in core−shell structures can also lead to the reduction in magnetization.[24] It has been reported that the saturation magnetization decreases with increasing particle size in $CoFe_2O_4$ nanoparticles synthesized by the chemical route.[59] This behavior is attributed to incomplete ferrite formation and the formation of an intermediate hydroxide phase like FeOOH due to an excess amount of Fe^{3+} at a higher alkali like NaOH. However, our studies show that the reduction in the magnetization with increasing particle size in $CoFe_2O_4$ nanoparticles is due to the presence of the nonmagnetic ferrihydrite phase, which is unambogusly confirmed by Raman spectroscopy. Therefore, nonmagnetic ferrihydrite formation from Fe^{3+} salt solutions leads to a decrease in saturation magnetization with digestion time. The decrease in saturation magnetization with digestion time is also confirmed from the Mossbauer spectroscopy by looking at the hyperfine splitting value at various digestion times. The hyperfine field value is directly related to the magnetization value.

D. Mossbauer Spectroscopy. The room temperature Mossbauer spectra of $CoFe_2O_4$ nanoparticles prepared at different digestion times (1, 5, 15, and 120 min) are shown in Figure 7. Experimental data are fitted with Lorentzian-shaped lines by the method of least squares. The Mossbauer parameters such as isomer shift (IS), quadruplet splitting (QS), hyperfine magnetic field $\langle B \rangle$, line width (Γ), and relative intensities I_{rel} for the nanocrystalline $CoFe_2O_4$ synthesized at different digestion times are given in Table 1. Distribution of Fe^{3+} in the A- and B-sites is determined by comparing the relative area covered

TABLE 1: Mossbauer Parameters Such As Isomer Shift (IS) Relative to That of α-Fe at 300 K, Quadruplet Splitting (QS), the Hyperfine Magnetic Field ⟨*B*⟩, Line Width (Γ), and Relative Intensities I_{rel} at 300 K for the Nanocrystalline $CoFe_2O_4$ Synthesized at Various Digestion Times

digestion time (min)	site	IS (mm/s)	*B* (Tesla)	QS (mm/s)	Γ (mm/s)	I_{rel} (%)
1	A	0.22	43.55	0.06	0.42	43.5
	B	0.33	46.79	0.03	0.42	46.8
5		0.35		0.78	0.42	6.9
	A	0.22	46.22	0.03	0.42	51.0
	B	0.33	42.39	−0.06	0.42	42.1
15		0.34		0.77	0.42	11.9
	A	0.22	41.61	−0.05	0.42	36.2
	B	0.33	45.80	−0.01	0.42	51.9
120		0.34		0.74	0.42	9.7
	A	0.22	43.02	0.00	0.42	39.9
	B	0.33	46.30	−0.04	0.42	50.4

by the sextets from the A- and B-sites. At 1-min digestion time, Fe^{3+} ions are equally distributed between A- and B-sites, and form the perfect inverse spinel structure with a large weighted hyperfine field value of 45 T. The corresponding Ms value is 60 emu/g. At higher digestion times, relative areas under the A- or B-sites are unequal and hence the Fe^{3+} ion can coordinate with the Co^{2+} ion through O. The measured value of isomer shift for Fe^{3+} in tetrahedral and octahedral sites is 0.22 and 0.33 mm/s, respectively. These are in good agreement with those previously reported values of $CoFe_2O_4$.[60] There is no significant change of isomer shift values by increased digestion time. This means that the *s* electron charge distribution of Fe ions is not influenced by enhanced digestion time. The quadruplet splitting values for sextuplets indicate that there is no electric field gradient generated with the change in the digestion time. At 5, 15, and 120 min digestion times, Mossbauer spectra consist of a superparamagnetic doublet apart from sextets. Relative area occupied by superparamgeitc doublet increases from 6.9 to 11.9 as the digestion time increases from 5 to 15 min. The presences of a doublet indicates the superparamagnetic size $CoFe_2O_4$ nanoparticles at higher digestion times. Apart from the superparamagnetic $CoFe_2O_4$ particles, formation of ferrihydrite from Fe^{3+} solution, at higher temperature during precipitation, can also lead to a doublet pattern. The magnetic ordering temperatures observed for the natural ferrihydrite ranges from 28 to 70 K.[49] These doublets are fitted with Lorentzian-shaped peaks with isomer shifts of 0.35 and 0.34 mm/s and quadruplet splitting of 0.78 and 0.77 mm/s, respectively. The nonzero quadruplet splitting values are in good agreement with the literature values of ferrihydrite.[61] In the case of superparamagnetic $CoFe_2O_4$ nanoparticles, the quadruplet splitting is 0.67 mm/s.[62] Therefore, the doublet pattern corresponds to the presence of ferrihydrite and superparamagnetic $CoFe_2O_4$ nanoparticles. The weighted average hyperfine field value is 44.3 and 43.7 T at digestion times of 5 and 15 min, respectively. At 120 min the weighted hyperfine field is 44.6 T and the relative area occupied by the doublet decreases to 9.7, with the isomer shift and quadruplet values of 0.34 and 0.74 mm/s, respectively. The result of a nonzero quadruplet splitting for the doublet indicates that the Fe in A- and B-sites are distorted from cubic symmetry. By contrast, the quadruplet splitting for the sextuplets is found to be small. This is often encountered in small particles, probably due to distortion, where axes are randomly oriented with respect to the direction of the hyperfine field, i.e., the direction of the Fe magnetization. The quadruplet splitting of 0.74 mm/s at 120 min digestion time indicates the presence of the ferrihydrite phase. Figure 8 shows a decrease in trend of weighted hyperfine field and saturation magnetization as a function of digestion time, which is consistent with our magnetization measurements data (Figure 5). The presence of a superparamagnetic doublet, along with sexlets with decreasing hyperfine field value, also confirms the presence of the superparamagnetic nature of $CoFe_2O_4$ nanoparticles and the presence of nonmagnetic ferrihydrite at higher digestion times.

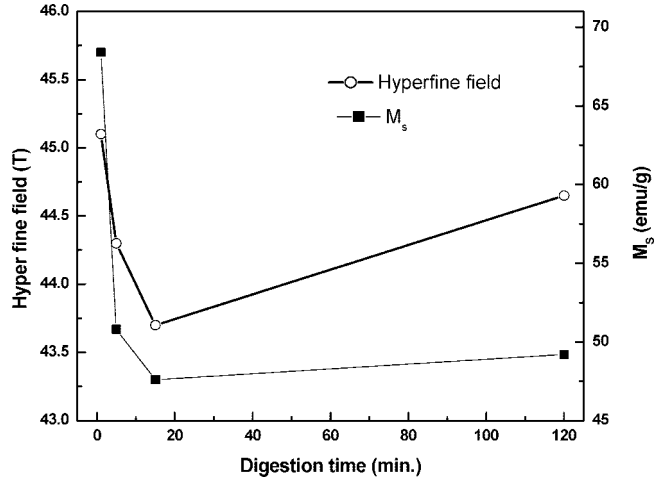

Figure 8. The variation of hyperfine field and saturation magnetization as a function of digestion time.

Conclusions

We have studied the effect of digestion time on size, distribution, impurity formation, and magnetic properties of $CoFe_2O_4$ nanoparticles synthesized by the coprecipitation method. Particle size increases from 14 to 19 nm as the digestion time increases from 1 to 120 min. Saturation magnetization of $CoFe_2O_4$ nanoparticles decreases with increasing digestion time. These results suggest that the dissolution of $Co^{2+}-Fe^{3+}$ complexes form the surface followed by crystallization of spinel oxide through Oswald ripening process. Nonmagnetic ferrihydrite formation from Fe^{3+} solution during precipitation is confirmed by Raman and Mossbauer spectroscopy. The presence of nonmagnetic ferrihydrite and larger particles due to the Oswald ripening process leads to a progressive decrease in saturation magnetization with higher digestion times. Superparamagnetic doublets apart from sextets in Mossbauer spectra of $CoFe_2O_4$, obtained at higher digestion time, confirm the presence of superparamagnetic size particles along with nonmagnetic ferrihydrite that causes the decrease in saturation magnetization. Our findings suggest that a digestion time of 1 min is sufficient to obtain $CoFe_2O_4$ nanoparticles with correct stoichiometry and chemical purity.

Acknowledgment. We thank P. Chandramohan and Dr. M. P. Srinivasan, the water and steam chemistry laboratory for Mossbauer spectroscopy and Raman experiments, and Dr. R. Divakar, Dr. E. Mohandas, and Dr. M. Vijayalakshmi for HRTEM data and analysis. We also thank Dr. T. Jayakumar and Dr. P. R.Vasudeva Rao for their support and encouragement.

References and Notes

(1) Georgescu, M.; Viota, J. L.; Klokkenburg, M.; Erne, B. H.; Vanmaekelbergh, D.; van Emmichoven, P. A. *Z. Phys. Rev. B* **2008**, *77*, 024423.

(2) Jordanovic, J.; Klapp, S. H. L. *Phys. Rev. Lett.* **2008**, *101*, 038302.

(3) Lisfi, A.; Williams, C. M.; Nguyen, L. T.; Lodder, J. C.; Coleman, A.; Corcoran, H.; Johnson, A.; Chang, P.; Kumar, A.; Morgan, W. *Phys. Rev. B* **2007**, *76*, 054405.

(4) Pileni, M. P. J. *Phys. Chem. C* **2007**, *111*, 9019.
(5) Rao, C. N. R.; Muller, A.; Cheetham, A. K. *The Chemistry of Nanomaterials*; Wiley-VCH: Weinheim, Germany, 2004; Vol. 1.
(6) Wang, X.; Zhuang, J.; Peng, Q.; Li, Y. *Nature Lett.* **2005**, *437*, 121.
(7) Alivisatos, A. P. *J. Phys. Chem.* **1996**, *100*, 13226.
(8) Burda, C.; Chen, X.; Narayanan, R.; El-Sayed, M. A. *Chem. Rev.* **2005**, *105*, 1025.
(9) Fontijn, W. F. J.; van der Zaag, P. J.; Devillers, M. A. C.; Brabers, V. A. M.; Metselaar, R. *Phys. Rev. B* **1997**, *56*, 5432.
(10) Wang, P.; Kakol, Z.; Wittenauer, M.; Honig, J. M. *Phys. Rev. B* **1990**, *42*, 4553.
(11) Sivakumar, N.; Narayanasamy, A.; Ponpandian, N.; Govindaraj, G. *J. Appl. Phys.* **2007**, *101*, 084116.
(12) Duthett, D.; Friedberg, S. A. *Phys. Rev.* **1961**, *121*, 1662.
(13) Philip, J.; Shima, P. D.; Raj, B. *Appl. Phys. Lett.* **2008**, *92*, 043108.
(14) Pankhurst, Q. A.; Connolly, J.; Jones, S. K.; Dobson, J. *J. Phys. D* **2003**, *36*, R167.
(15) Philip, J.; Rao, C. B.; Jayakumar, T.; Raj, B. *NDT&E Int.* **2000**, *33*, 289.
(16) Philip, J.; Jaykumar, T.; Sundaram, P. K.; Raj, B. *Meas. Sci. Technol.* **2003**, *14*, 1289.
(17) Philip, J.; Gnanaprakash, G.; Jayakumar, T.; Sundaram, P. K.; Raj, B. *Macromolecule* **2003**, *36*, 9230.
(18) Cullity, B. D. *Introduction to magnetic materials*; Addision-Wesley: New York, 1972.
(19) Philip, J.; Gnanaprakash, G.; Panneerselvam, G.; Antony, M. P.; Jayakumar, T.; Raj, B. *J. Appl. Phys.* **2007**, *102*, 1.
(20) Rozenberg, G. Kh.; Amiel, Y.; Xu, W. M.; Pasternak, M. P.; Jeanloz, R.; Hanfland, M.; Taylor, R. D. *Phys. Rev. B* **2007**, *75*, 20102(R)
(21) Stewart, S. J.; Figueroa, S. J. A.; Lopez, J. M. R.; Marchetti, S. G.; Bengoa, J. F.; Prado, R. J.; Requejo, F. G. *Phys. Rev. B* **2007**, *75*, 073408.
(22) Hu, G.; Choi, J. H.; Eom, C. B.; Harris, V. G.; Suzuki, Y. *Phys. Rev. B* **2000**, *62*, R779.
(23) Kuckelhaus, S.; Garcia, V. A. P.; Lacava, L. M.; Azevedo, R. B.; Lacava, Z. G. M.; Lima, E. C. D.; Figueiredo, F.; Tedesco, A. C.; Morais, P. C. *J. Appl. Phys.* **2003**, *93*, 6707.
(24) Tung, L. D.; Kolesnichenko, V.; Caruntu, D.; Chou, N. H.; Ocornnor, C. J.; Spinu, L. *J. Appl. Phys.* **2003**, *93*, 7486.
(25) Moumen, N.; Bonville, P.; Pileni, M. P. *J. Phys. Chem.* **1996**, *100*, 14410.
(26) Bhame, D. S.; Joy, P. A. *J. Appl. Phys.* **2006**, *100*, 113911.
(27) Liu, B. H.; Ding, J. *Appl. Phys. Lett.* **2006**, *88*, 042506.
(28) Kim, K. J.; Lee, H. S.; Lee, M. H.; Lee, S. H. *J. Appl. Phys.* **2002**, *91*, 9974.
(29) Tailhades, P.; Bonningue, C.; Rousset, A.; Bouet, L.; Pasquet, I.; lebryun, S. *J. Magn. Magn. Mater.* **1999**, *193*, 148.
(30) Tedesco, A. C.; Oliveira, D. M.; Lacava, Z. G. M.; Azevedo, R. B.; Lima, E. C. D.; Gansau, C.; Buske, N.; Morais, P. C. *J. Appl. Phys.* **2003**, *93*, 6704.
(31) Jeppson, P.; Sailer, R.; Jarabek, E.; Sandstrom, J.; Anderson, B.; Bremer, M.; Grier, D. G.; Schulz, D. L.; Caruso, A. N. *J. Appl. Phys.* **2006**, *100*, 114324.
(32) Shafi, K. V. P. M.; Gedanken, A.; Prozorov, R.; Balogh, J. *Chem. Mater.* **1998**, *10*, 3445.
(33) Lee, D. K.; Kim, Y. H.; Kang, Y. S.; Stroeve, P. *J. Phys. Chem. B* **2005**, *109*, 14939.
(34) Song, Q.; Zhang, Z. J. *J. Phys. Chem. B* **2006**, *110*, 11250.
(35) Liu, B. H.; Ding, J.; Dong, Z. L.; Boothroyd, C. B.; Yin, J. H.; Yi, J. B. *Phys. Rev. B* **2006**, *74*, 184427.
(36) Zhao, S-Y.; Qiao, R.; Zhang, X. L.; Kang, Y. S. *J. Phys. Chem. C* **2007**, *111*, 7875.
(37) Gnanaprakash, G.; Philip, J.; Jayakumar, T.; Raj, B. *J. Phys. Chem. B* **2007**, *111*, 7978.
(38) Mullin, J. W. *Crystallisation*; Butterworth & Co Publishers Ltd: London, UK, 1972.
(39) Tiemann, M.; Marlow, F.; Hartikainen, J.; Weiss, O.; Linden, M. *J. Phys. Chem. C* **2008**, *112*, 1463.
(40) Jolivet, J.-P.; Tronc, E.; Chaneac, C. *C. R. Chim.* **2002**, *5*, 659.
(41) Si, S.; Li, C.; Yu, D.; Peng, Q.; Li, Y. *Cryst. Growth Des.* **2005**, *5*, 391.
(42) Narayanan, R.; El-Sayed, M. A. *J. Phys. Chem. B* **2005**, *109*, 12663.
(43) Chen, Y.; Kim, M.; Lian, G.; Johnson, M. B.; Peng, X. *J. Am. Chem. Soc.* **2005**, *127*, 13331.
(44) Huang, F.; Banfield, J. F. *J. Am. Chem. Soc.* **2005**, *127*, 4523.
(45) Djerdjev, A. M.; Beattie, J. K. *Langmuir* **2008**, *24*, 7711.
(46) Yin, M.; O'Brien, S. *J. Am. Chem. Soc.* **2003**, *125*, 10180.
(47) Oskam, G.; Nellore, A.; Penn, R. L.; Searson, P. C. *J. Phys. Chem. B* **2003**, *107*, 1734.
(48) Lifshitz, I. M.; Slyozov, V. V. *J. Phys. Chem. Solids* **1961**, *19*, 35.
(49) Jambor, J. L.; Dutrizac, J. E. *Chem. Rev.* **1998**, *98*, 2549.
(50) Drits, V. A.; Sakharov, B. A.; Salyn, A. L.; Manceau, A. *Clay Miner.* **1993**, *28*, 185.
(51) Dediu, V.; Ferdeghini, C.; Matacotta, F. C.; Nozar, P.; Ruani, G. *Phys. Rev. Lett.* **2000**, *84*, 4489.
(52) Yu, T.; Shen, Z. X.; Shi, Y.; Ding, J. *J. Phys.: Condens. Matter* **2002**, *14*, L613.
(53) Gasparov, L. V.; Tanner, D. B.; Romero, D. B.; Berger, H.; Margaritondo, G.; Forro, L. *Phys. Rev. B* **2000**, *69*, 7939.
(54) Mazzetti, L.; Thistlethwaite, P. J. *J. Raman Spectrosc.* **2002**, *33*, 104.
(55) Janney, D. E.; Cowley, J. M.; Buseck, P. R. *Am. Mineral.* **2001**, *86*, 327.
(56) de Faria, D. L. A.; Silva, S. V.; deOliveira, M. T. *J. Raman Spectrosc.* **1997**, *28*, 873E878.
(57) Makhlouf, S. A.; Parker, F. T.; Spada, F. E.; Berkowitz, A. E. *J. Appl. Phys.* **1997**, *81*, 5561.
(58) Goya, G. F.; Rechenberg, H. R. *J. Magn. Magn. Mater.* **1991**, *196*, 191.
(59) Chinnasamy, C. N.; Jeyadevan, B.; Perales-Perez, O.; Shinoda, K.; Tohji, K.; Kasuya, A. *IEEE Trans. Magn.* **2002**, *38*, 2640.
(60) Greenwood, N. N.; Gibb, T. C. *Mossbauer spectroscopy*; Chapman and Hall Ltd: London, UK, 1971.
(61) Murad, E. *J. Magn. Magn. Mater.* **1988**, *74*, 153.
(62) Moumen, N.; Bonville, P.; Pileni, M. P. *J. Phys. Chem.* **1996**, *100*, 14410.

JP8083875